Spin yields of neutron-rich nuclei from deep inelastic reactions

S. J. Asztalos, I. Y. Lee, K. Vetter, B. Cederwall, R. M. Clark, M. A. Deleplanque, R. M. Diamond, P. Fallon, K. Jing, L. Phair, A. O. Macchiavelli, J. O. Rasmussen, F. S. Stephens, and G. J. Wozniak
Nuclear Science Division, Lawrence Berkeley National Laboratory, Berkeley, California 94720

J. A. Becker, L. A. Bernstein, and D. P. McNabb
Physics Division, Lawrence Livermore National Laboratory, Livermore, California 94550

P. F. Hua and D. G. Sarantites
Washington University, St. Louis, Missouri 63130

J. X. Saladin
University of Pittsburgh, Pittsburgh, Pennsylvania 15260

C.-H. Yu
University of Rochester, Rochester, New York 14627

J. A. Cizewski
Rutgers University, New Brunswick, New Jersey 08903

R. Donangelo
Instituto de Física, Universidade Federal do Rio de Janeiro, Rio de Janiero, Brazil
(Received 15 April 1999; published 8 September 1999)

The potential for using deep inelastic reactions to populate high-spin states in neutron-rich nuclei is studied in a series of experiments using GAMMASPHERE for γ-ray detection and a silicon strip detector for measuring the angles of projectilelike and targetlike fragments. In three experiments 61 new transitions up to a maximum spin of $22\hbar$ in 12 neutron-rich rare-earth nuclei were found. We observe that γ-ray yields as a function of spin are flatter for all neutron transfer products than for inelastic excitation of either the projectile or target nucleus. Calculations are presented which indicate that this difference cannot be accounted for by quasielastic processes, but more likely are the result of larger energy loss processes, such as deep inelastic reactions. [S0556-2813(99)06009-4]

PACS number(s): 21.10.Re, 25.70.Lm, 25.70.Hi, 21.60.Ev

I. INTRODUCTION

The ability of the deep inelastic mechanism to generate large amounts of rotational angular momentum has long been recognized [1]. Using a γ-ray multiplicity detector Glässel *et al.* were able to demonstrate γ-ray multiplicities in excess of 15 in the reaction ^{20}Ne+^{nat}Ag at 175 MeV [2]. As might be expected with a more massive projectile and higher bombarding energies, the maximum γ-ray multiplicities were shown to exceed 30 in a series of reactions involving ^{86}Kr+^{107,109}Ag, ^{165}Ho, and ^{197}Au, all at 618 MeV [3]. These experiments were primarily concerned, however, with relaxation time scales of the deep inelastic mechanism. Takai *et al.* were among the first to utilize discrete γ-ray spectroscopy in the study of deep inelastic reactions [4]. In that experiment Doppler corrections were made to γ rays emitted from recoiling targetlike nuclei and spin states as high as $20\hbar$ were resolved. In a recent paper [5] we extended this technique to neutron-rich nuclei which, because of neutron evaporation or the unavailability of stable beam-target combinations, cannot be populated by more conventional techniques such as compound nucleus formation. In an experiment using ^{48}Ca+^{176}Yb at 250 MeV we found new γ-ray transitions in several neutron-rich Yb isotopes. These results allowed us to address questions regarding the structure of neutron-rich nuclei at high spins.

Here we extend the scope of our previous work by addressing the topic of spin production as a function of the masses of the projectile and target. Knowledge of the behavior of these parameters is desirable for optimizing the spin yield of very neutron-rich nuclei. We accomplish this by studying several reactions that have an isotope (beam or target) common to successive experiments. Our second experiment, ^{154}Sm+^{176}Yb at 949 MeV, had ^{176}Yb in common with the reaction ^{48}Ca+^{176}Yb, while the third experiment, ^{154}Sm+^{208}Pb at 1 GeV, had ^{154}Sm in common with the second experiment. All three experiments were conducted at projectile energies roughly 20% above their respective Coulomb barriers. Although several features of the experiment ^{48}Ca+^{176}Yb were discussed in our previous paper [5], a discussion of the spin yields from that experiment was postponed so that it could be compared with the spin yields from the two remaining experiments in this paper.

In Sec. II the experimental setup is discussed. In Sec. III we discuss the reaction kinematics and the role it plays in particle identification, as well as the techniques used to de-

TABLE I. Distance from the target to the center of the silicon strip detector, angles subtended by the silicon strip detector, and grazing angle for the indicated reactions.

	d [cm]	Angular range [deg]	Grazing angle [deg]
^{48}Ca+^{176}Yb	2.0	55–67	65
^{154}Sm+^{176}Yb	1.0	45–63	53
^{154}Sm+^{208}Pb	1.0	45–65	55

rive the spin yields. Section IV A presents level schemes of the rare-earth nuclei for which new γ-ray transitions have been found. Experimental spin yields reflect the ability of the projectile to transfer angular momentum to the various reaction products. Spin yields based on γ-ray intensities are presented in Sec. IV B, and are then compared to quasielastic transfer calculations in Sec. IV C.

In a companion paper [6] we present isotopic yield results for all three experiments.

II. EXPERIMENTAL METHODS

The experiments described in this paper were performed at the 88-Inch Cyclotron at the Lawrence Berkeley National Laboratory. Gamma rays were detected by the GAMMASPHERE array, which for ^{154}Sm+^{176}Yb and ^{154}Sm+^{208}Pb had 55 high-purity Compton-suppressed germanium detectors. For ^{154}Sm+^{176}Yb two stacked targets (each 0.5 mg/cm^2 thick and enriched to 97.8% ^{176}Yb) were used, while for ^{154}Sm+^{208}Pb a single target (1 mg/cm^2 thick and enriched to 99.9% ^{208}Pb) was used. These targets were sufficiently thin that γ-ray emission occurred after the recoiling fragments left the target. The direction of the recoiling fragments was recorded by a silicon strip detector electrically segmented into 16 concentric rings on its front face and 16 wedges in the ϕ direction on the back face. Signal multiplexing in the electronics allowed for complete angular identification based on only 20 output signals; however, two-body kinematics allows only one ϕ segment to fire per quadrant. This permitted additional signal multiplexing so that only 12 analog-to-digital converters were required. The silicon strip detector was placed inside the 14-in.-diam target chamber with the beam axis serving as the centerline of the detector. The distance from target to detector was determined by the requirement that the calculated grazing angle [7] fall roughly between the inner and outer radii of the silicon strip detector. The distance from the target to the center of the silicon strip detector, the angles subtended by the silicon strip detector, and the grazing angle for each reaction are given in columns 2, 3, and 4 of Table I.

In each experiment, an event was defined as the detection of at least one particle at the silicon strip detector in coincidence with two γ rays recorded by GAMMASPHERE. Under these conditions the event rate was approximately 1 kHz. Furthermore, particle-γ-γ-γ events comprised nearly a quarter of the data which made it possible to analyze both γ-γ and γ-γ-γ coincidences.

TABLE II. Kinematic ranges of the projectilelike and targetlike nuclei. The labels are to be interpreted as follows: for a projectilelike (targetlike) fragment, $\theta_{\rm pl}$ ($\theta_{\rm tl}$) refers to the angles over which the projectilelike (targetlike) fragment will hit the silicon strip detector if the targetlike (projectilelike) fragment, recoiling over the range $\theta_{\rm tl}$, ($\theta_{\rm pl}$) is to miss it. Similar interpretations hold for the labels $E_{\rm pl}$ and $E_{\rm tl}$. For ^{48}Ca+^{176}Yb and ^{154}Sm+^{208}Pb the projectilelike fragment always has higher energy when hitting the silicon strip detector, thus making particle identification possible. By contrast, for ^{154}Sm+^{176}Yb it is only when both projectilelike and targetlike fragments hit the silicon strip detector that the kinematics are separable.

Expt.	Part. detected	$\theta_{\rm pl}$ [deg]	$\theta_{\rm tl}$ [deg]	$E_{\rm pl}$ [MeV]	$E_{\rm tl}$ [MeV]
^{48}Ca+^{176}Yb	projectilelike	57–67	49–55	178–195	55–72
	targetlike	37–55	56–67	197–224	26–53
^{154}Sm+^{176}Yb	projectilelike	49–63	33–45	283–474	475–667
	targetlike	29–45	48–63	461–666	283–488
^{154}Sm+^{208}Pb	projectilelike	53–65	36–45	367–518	472–633
	targetlike	29–44	52–65	638–825	175–362

III. EXPERIMENTAL TECHNIQUES

Detection of one of the recoiling particles at the silicon strip detector, in conjunction with the assumption of two-body kinematics, allows the velocity vectors of both projectilelike and targetlike fragments to be calculated. The intrinsic energy resolution of the silicon strip detector was quickly degraded by radiation damage from ion bombardment; hence direct energy loss measurements were not possible. Nonetheless, the recoiling projectilelike and targetlike fragments could still be distinguished kinematically from one another (except in the experiment ^{154}Sm+^{176}Yb).

In the ^{48}Ca+^{176}Yb and ^{154}Sm+^{208}Pb experiments it was possible to distinguish between projectilelike and targetlike fragments hitting the detector due to the large difference in energy between the two fragments over the angular range of the silicon strip detector, as is illustrated in Table II. Accordingly, there were only two possibilities for carrying out the Doppler correction of each γ ray — either assuming that the fragment hitting the silicon strip detector emitted the γ ray or by assuming the other fragment emitted the γ ray. For the case where the Doppler correction is appropriate for a γ ray emitted by the projectilelike fragment (targetlike fragment), a γ ray emitted by the targetlike fragment (projectilelike fragment) has the wrong Doppler correction applied to it. This technique therefore has the desirable effect of smearing out the inappropriate kinematic solution. For ^{154}Sm+^{176}Yb the energy ranges of the projectilelike and targetlike fragments overlap over the angles subtended by the silicon strip detector, leaving four possibilities for carrying out the Doppler correction of each γ ray.

In each experiment the Doppler-corrected γ rays were then incremented into γ-γ matrices and γ-γ-γ cubes created for each distinct kinematic solution. The data were analyzed using the RADWARE packages [8]. Both analysis packages allow for the placement of one or more gates on known transitions and the generation of coincident spectra. The re-

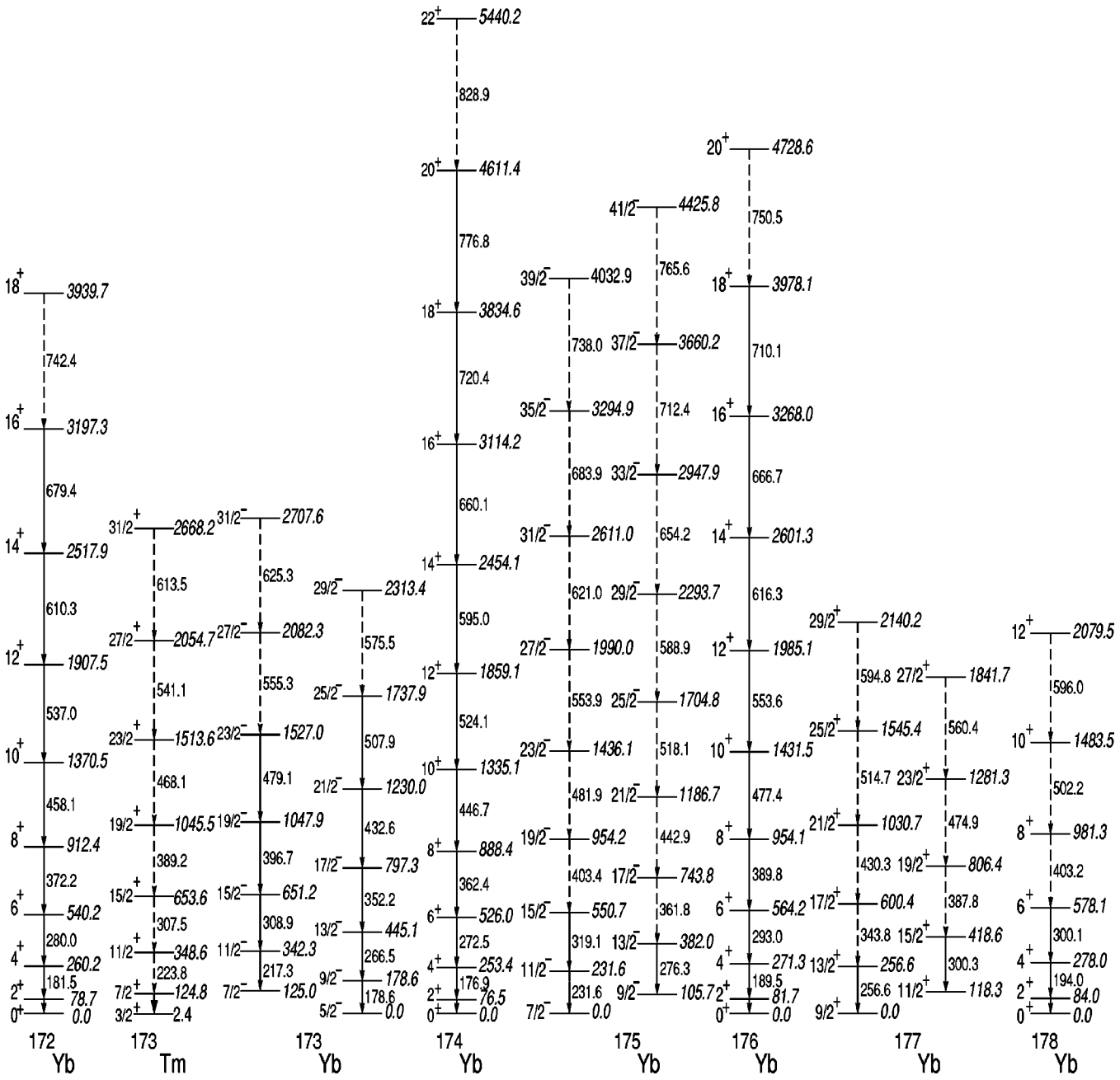

FIG. 1. Level schemes, including γ-ray and level energies, plus tentative spin and parity assignments, for Yb-like nuclei. Transitions denoted by a solid arrow represent those known prior to this work [12], while the dashed arrows represent those added by experiments ^{48}Ca+^{176}Yb and ^{154}Sm+^{176}Yb. $\Delta I=1$ crossover transitions between signature partners in odd-A nuclei are not shown.

sultant spectra were then analyzed for evidence of new transitions. This analysis resulted in the level schemes of Figs. 1 and 2 for Yb- and Sm-like nuclei, respectively.

Spin yields were generated by singly or doubly gating on the lowest possible transition(s) in a nucleus in order to resolve weak, higher-lying transitions from the background. While a gate on any member of a cascade might suffice for resolving the cascade, in practice the lowest possible transition is chosen as a gate since all transitions below the gate are restricted to having an intensity equal to the intensity of the gated transition and thus do not reflect the true yield. In a few cases where a single gate in twofold data could not produce a clean spectrum, double gates were placed on the two lowest members of a rotational cascade in threefold data. The following strategy of summing spectra was employed in instances when one (single or double) gate could not adequately resolve the highest transitions: assuming that the intensity of the nth transition has been obtained by one (single or double gate), while the intensity of the nth+1 transition is too weak to measure, a sum of m gates all below the nth transition is used. The ratio of the intensity of the nth transition in this multiply gated spectrum to that obtained

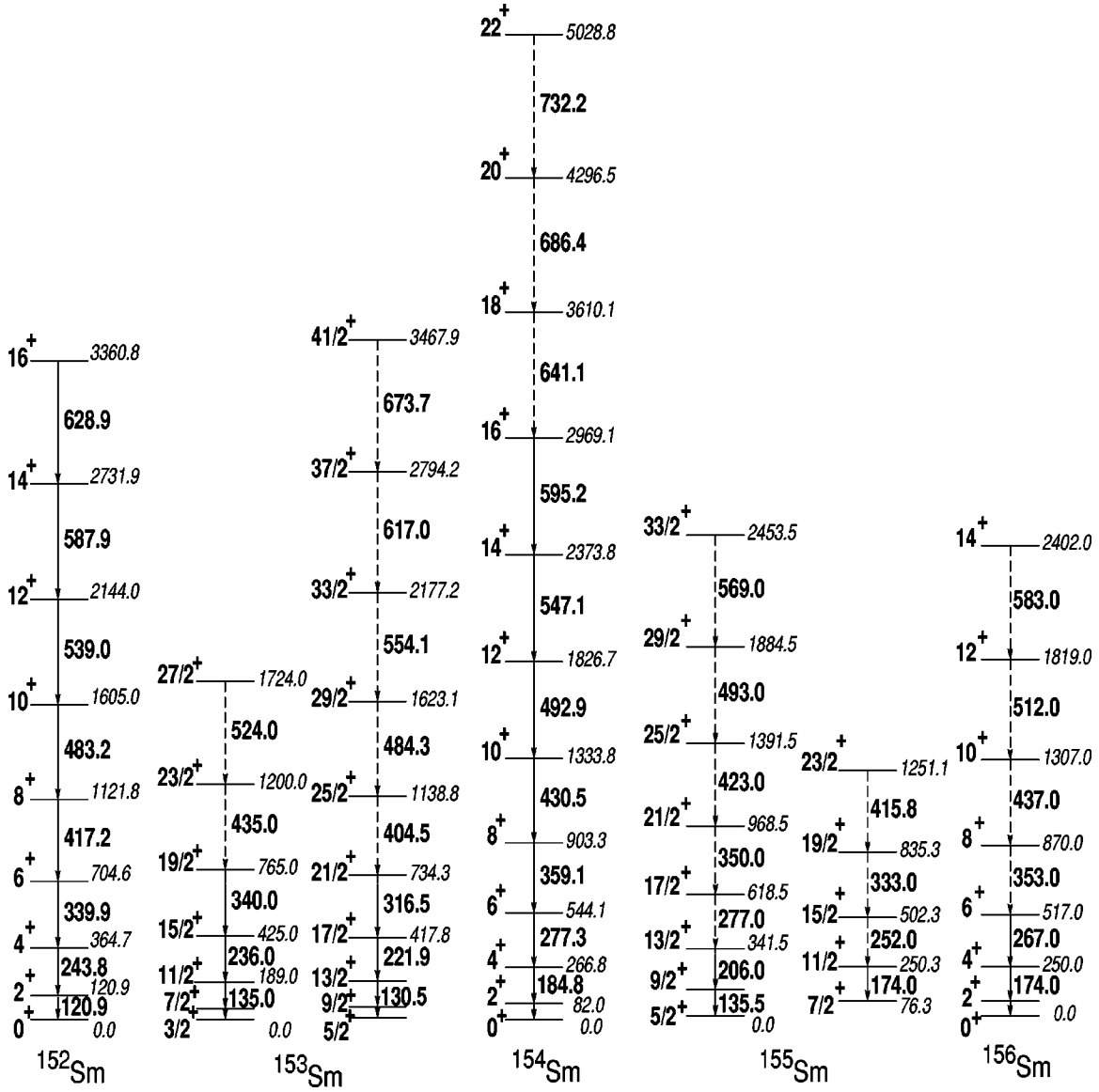

FIG. 2. Level schemes for Sm isotopes from the experiments ^{154}Sm+^{176}Yb and ^{154}Sm+^{208}Pb. See the caption to Fig. 1 for interpretation.

from one (single or double gate) gives a normalization factor that is applied to the nth+1 and all higher transitions in the multiply gated spectrum. Peak areas were extracted by fitting the peaks with a Gaussian shape and a constant background. To convert from areas to intensities it was necessary to correct for the relative efficiency of GAMMASPHERE. Applying these methods produced the spin yield curves in Figs. 3 and 4 for Yb and Sm nuclei, respectively.

Of particular interest is the effect on the spin yields when one of the reaction partners is changed. To make this comparison, relative intensities from different reactions must be normalized. In the bottom plot of Fig. 5 the spin yields for all Yb isotopes are normalized by requiring that the intensities of the $6^+ \rightarrow 4^+$ transitions in ^{176}Yb (produced in either ^{48}Ca+^{176}Yb or ^{154}Sm+^{176}Yb) be identical. A similar normalization for Sm isotopes using the $6^+ \rightarrow 4^+$ transitions in ^{154}Sm resulted in the upper plot in the same figure.

IV. RESULTS AND DISCUSSION

One of the goals of our high-spin studies in the rare-earth region is to populate nuclei with sufficient angular momentum that the first backbend is observed [9]. From these data it would be possible to extract the interaction matrix element V, which is a measure of the strength of the Coriolis operator connecting the ground and excited states in the presence of pairing [5,10]. For heavy even-even rare-earth nuclei the backbend is predicted to lie around spin $20\hbar$ and at higher spins as additional neutrons are added [11]. We were able to populate states as high as 22^+ (^{174}Yb) in the ^{48}Ca+^{176}Yb reaction. Unexpectedly, higher-spin states were not observed when a heavier projectile was used — the highest observed spin using a Sm projectile was again 22^+ (^{154}Sm) in ^{154}Sm+^{208}Pb. We attribute this result, in part, to the appreciable Doppler broadening of the peak widths due to the large ($\beta \approx 0.1c$) recoil velocities of both the projectilelike

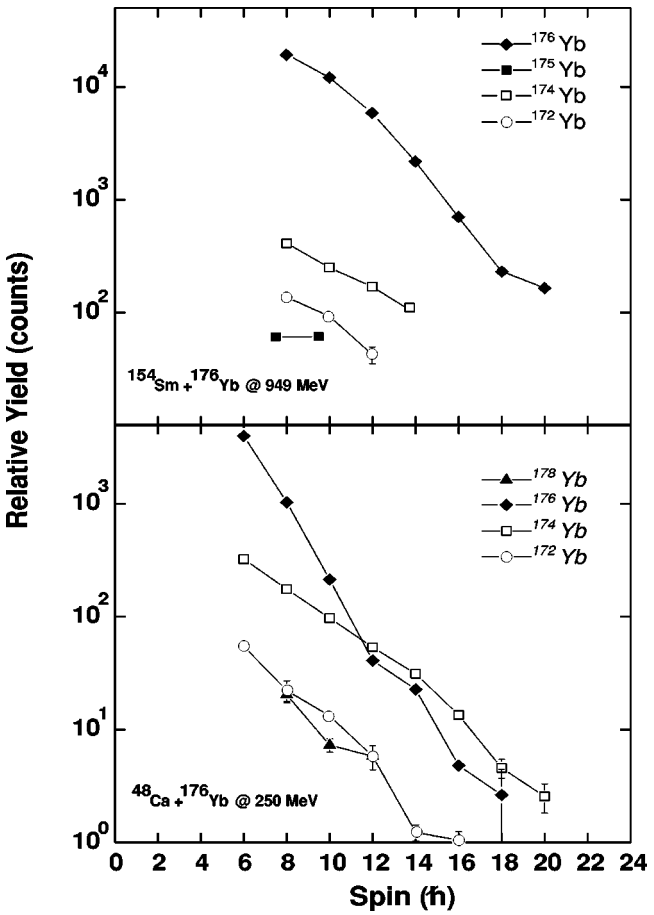

FIG. 3. Yb yrast spin yields from ^{48}Ca+^{176}Yb (lower) and ^{154}Sm+^{176}Yb (upper). The data corresponding to ^{48}Ca+^{176}Yb were obtained from single gates of twofold data, while the data from ^{154}Sm+^{176}Yb comes from double gates of threefold data.

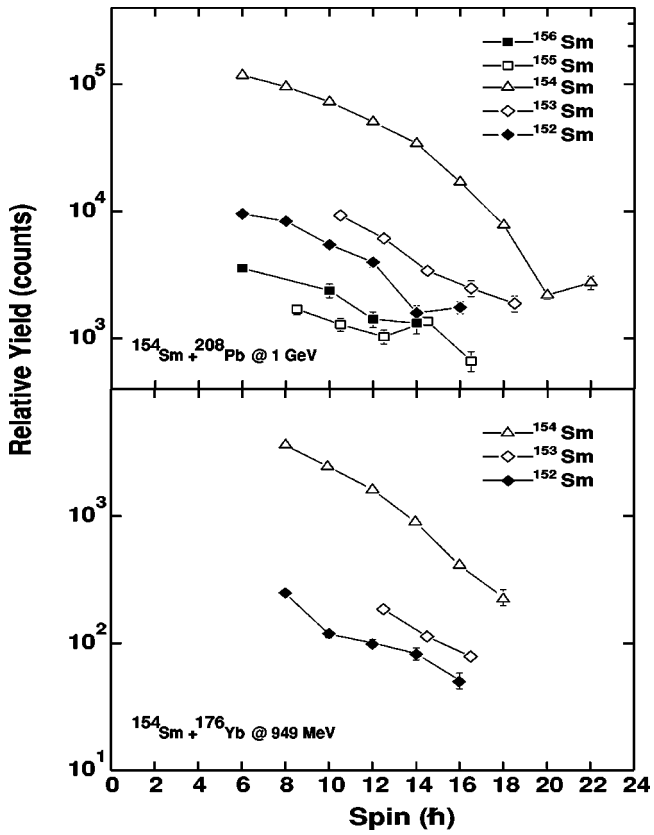

FIG. 4. Sm yrast spin yields from ^{154}Sm+^{176}Yb (lower) and ^{154}Sm+^{208}Pb (upper). The data corresponding to ^{154}Sm+^{176}Yb come from double gates of threefold data, while the data for ^{154}Sm+^{208}Pb were obtained from single gates of twofold data.

and targetlike fragments in that experiment. The inability to separate the kinematic solutions in ^{154}Sm+^{176}Yb added significantly to the background and obscured weaker, high-lying transitions. Another contributing factor is the presence of numerous strong transitions from octupole bands to states in the yrast band, which tend to dominate the spectrum above 750 keV in the even-even Sm isotopes [12]. In spite of these limitations a total of 61 new transitions were added to the level schemes of 12 rare-earth nuclei from these three experiments.

A. New levels

Based on our analysis, a total of 39 new transitions were added to the level schemes of one thulium and seven Yb isotopes populated in either ^{48}Ca+^{176}Yb or ^{154}Sm+^{176}Yb. A majority (30) of these new transitions are associated with ^{173}Tm, ^{175}Yb, ^{177}Yb, or ^{178}Yb — odd-*A* and/or unstable nuclei. The high-spin states of such nuclei have been inaccessible via other reaction mechanisms.

Twenty-two new transitions were added to the level schemes of four Sm isotopes populated in either ^{154}Sm+^{176}Yb or ^{154}Sm+^{208}Pb. A large majority (19) of these new transitions are again associated with the odd-*A* and/or unstable nuclei ^{153}Sm, ^{155}Sm, and ^{156}Sm. The results for ^{156}Sm confirm the recent findings from spectroscopy of fission fragments [13].

B. Experimental spin yields

Spin yields, which measure population intensities as a function of spin, reflect the ability of a reaction mechanism to generate angular momentum. One notable feature of the spin yield curves is the decided change to a flatter slope for inelastic excitation of the zero-nucleon transfer product ^{176}Yb from ^{48}Ca+^{176}Yb around spin $12\hbar$, as seen in Fig. 3. (There is evidence of this same behavior above $20\hbar$ in the spin yield curve of ^{154}Sm from ^{154}Sm+^{208}Pb data shown in Fig. 4.) By contrast, the spin yield slopes of the transfer products ^{172,174,178}Yb are flatter over their entire spin range. Referring again to Fig. 3, one observes that the slopes of the spin yields for the transfer data are similar to the slope for ^{176}Yb data above $12\hbar$. This similarity suggests that the same mechanism is responsible for the flatter slopes of high-spin states in both the zero- and multiple-neutron transfer products. In the next section we show that quasielastic excitation alone cannot account for the shallower slopes in either of these cases.

We now address the normalized spin yields for Yb data from Fig. 5 to compare spin yields from successive experiments. The spin yield of ^{176}Yb from ^{154}Sm+^{176}Yb data falls

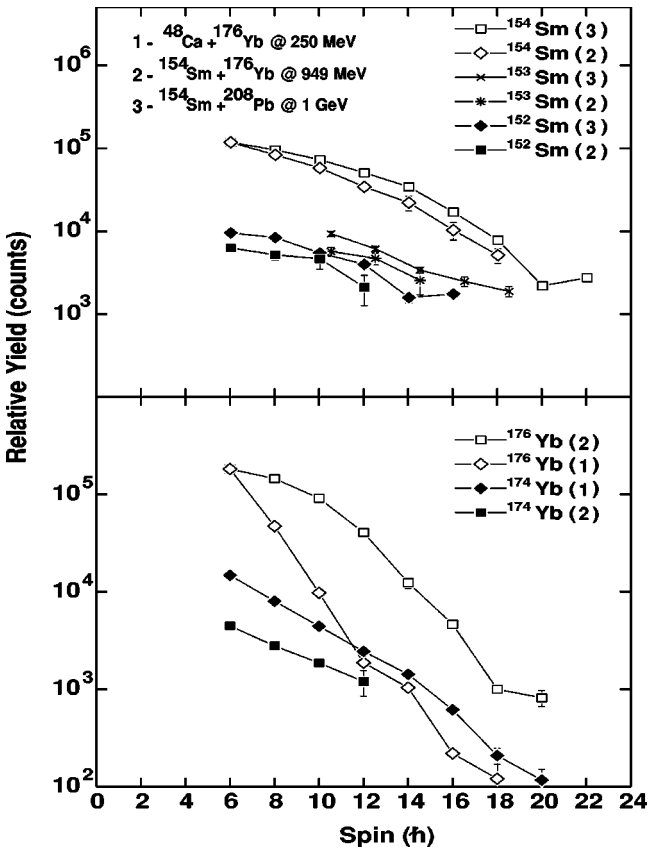

FIG. 5. A comparison of Yb and Sm normalized experimental yrast spin yields from the deep inelastic reactions. See the text for a discussion of the normalization method. The numbers in parentheses refer to the reaction from which the yield was derived. The lower figure compares Yb yields from the ^{48}Ca+^{176}Yb and ^{154}Sm+^{176}Yb reactions, while the upper figure makes the same comparison for Sm yields from the ^{154}Sm+^{176}Yb and ^{154}Sm+^{208}Pb reactions. All yields in this plot were obtained from γ-γ-γ coincidences.

much more slowly than it does in the ^{48}Ca+^{176}Yb data. We attribute this to the greater Coulomb excitation afforded by the higher atomic number of the Sm beam. A flatter slope is also seen in the two-neutron transfer product ^{174}Yb in the ^{154}Sm+^{176}Yb data. This is the result of feeding at higher spins in the ^{154}Sm+^{176}Yb reaction. However, the magnitude of the spin yield curve for ^{174}Yb in the ^{154}Sm+^{176}Yb data lies below that of the spin yield curve for ^{174}Yb in the ^{48}Ca+^{176}Yb data at all spins. This observation and the lack of measurable intensity above the 12^+ transition in the ^{154}Sm+^{176}Yb data have a common explanation, namely, the poorer γ-ray energy resolution in the ^{154}Sm+^{176}Yb data described above.

In the top plot of Fig. 5, where we make this same comparison for successive experiments involving Sm, we note that the slopes of the spin yield curves for the transfer products (^{152}Sm, ^{153}Sm) are quite similar, reflecting the basic similarity in experimental conditions and projectile-target combinations in the ^{154}Sm+^{176}Yb and ^{154}Sm+^{208}Pb experiments. Furthermore, the magnitude of the spin yields of ^{154}Sm from ^{154}Sm+^{208}Pb data is only slightly greater over the entire spin range than those from the ^{154}Sm+^{176}Yb data, which is likely due to the marginally greater Coulomb excitation from the larger atomic number of the lead target. The magnitude of the spin yields of ^{152}Sm and ^{153}Sm is also slightly higher in the ^{154}Sm+^{208}Pb data. This behavior is likely a consequence of the greater N/Z ratio of the target in the ^{154}Sm+^{208}Pb reaction, which leads to more neutron transfer, on average.

Our experimental results are in approximate agreement with those from an early experiment combining γ-ray spectroscopy from deep inelastic reactions and kinetic energy loss measurements, using the reaction ^{20}Ne+^{170}Er at 175 MeV [4]. By placing gates on γ-ray transitions in each of the Yb isotopes produced by nucleon transfer and subsequent evaporation and studying the ^{18}O particle kinetic energy spectrum the authors of that paper were able to correlate energy loss in the reaction with the gradual flattening of the spin yields for successively lighter Yb isotopes. Differences do exist, however. In our data the yield curves show a degree of flatness even in the zero-nucleon transfer products (at high spins), whereas this same behavior does not manifest itself until α transfer plus multiple-neutron evaporation occurred in the ^{20}Ne+^{170}Er data. Based on this observation, it appears that in our reactions the deep inelastic mechanism is activated with less nucleon transfer even though all three reactions occurred at significantly lower energies relative to the Coulomb barrier. This can perhaps be explained by their use of a lighter projectile, which may cause the reaction to be more direct-reaction-like up to a certain threshold energy loss experienced by the projectile-target pair, at which point the doorway to more complex reaction mechanisms is opened.

C. Theoretical spin yields

To model the contribution of the quasielastic component to the zero- and two-neutron transfer spin yields we employ a multiparticle-rotor model [14,15] written for calculating pair-transfer probabilities in deformed heavy ion reactions near the Coulomb barrier. This model, which uses a Nilsson basis to generate the rotational wave function of the target, takes into account Coulomb excitation and calculates pair-transfer probabilities at discrete points over the trajectory of the projectile. A theoretical description of these codes is given elsewhere [16,17]. These calculations are expected to model accurately the shape of the quasielastic component to the spin yields but cannot account for the absolute magnitude of spin yields, since inelastic transfer is modeled by an optical potential (i.e., no dissipation). We then ascribe differences between the calculations and experimental data to deep inelastic components of the total cross section.

The codes, previously applied only to head-on collisions, were modified for this analysis in an attempt to model grazing collisions appropriate to these experiments. To do this, the distance of closest approach corresponding to scattering into the grazing angle for the reaction was calculated. From this distance an effective atomic number of the target and effective bombarding energy of the projectile were computed. In order to compare the theoretical results with experi-

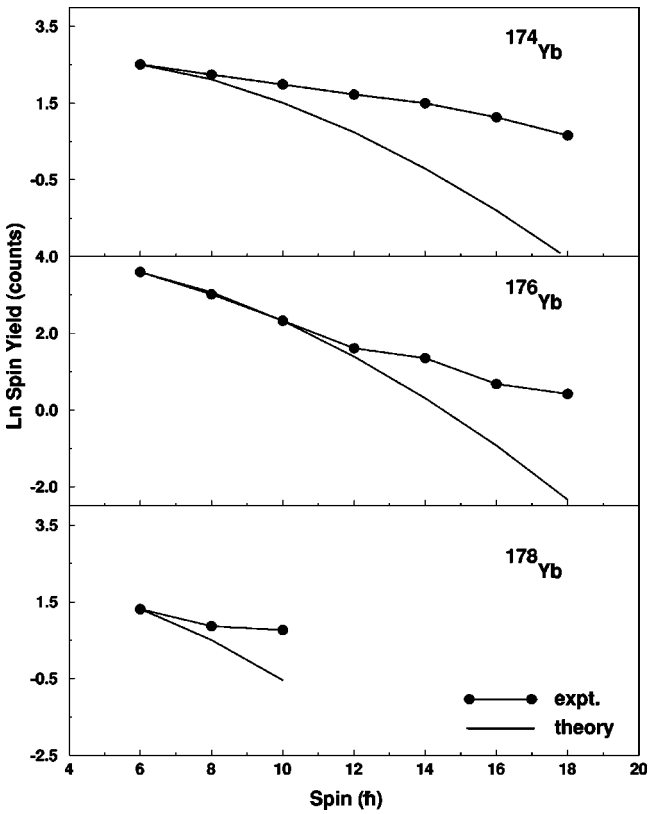

FIG. 6. A comparison of experimental and theoretical yrast spin yields for ^{174,176,178}Yb from the reaction ^{48}Ca+^{176}Yb. The top plot shows the results of the two-neutron transfer product ^{174}Yb, while the middle plot compares data on the inelastic excitation of the target nucleus. The bottom plot is the same as the top plot but for the two-neutron transfer product ^{178}Yb. All data points have been normalized at a spin of 6^+.

mental data on the yrast band, the population of the excited bands was cascaded down to the yrast band by making reasonable assumptions about the statistical versus collective ($E2$) branching ratios. The codes were run for ^{174}Yb, ^{176}Yb, and ^{178}Yb produced in the ^{48}Ca+^{176}Yb reaction since this reaction not only provided the best γ-ray energy resolution but also because the kinematics were uniquely defined.

The results are presented in Fig. 6, where it is readily observed that the calculations reproduce the shape of the inelastic yields in ^{176}Yb up to a spin of $12\hbar$. Beyond this point, however, the experimental yields fall more slowly. Theory also overestimates the slopes of the yield curves for two-neutron transfer into and out of ^{176}Yb, as is seen in the bottom and top plots of this figure. This suggests that at 20% above the barrier quasielastic excitation alone is insufficient to generate the observed higher spin yields, and that deep inelastic processes are making important contributions.

V. CONCLUSIONS

The relative flatness of the spin yield curves for neutron-transfer products from the reactions ^{48}Ca+^{176}Yb, ^{154}Sm+^{176}Yb, and ^{154}Sm+^{208}Pb suggests that the predominant contribution to the population of high-angular-momentum states is from processes other than quasielastic ones. This behavior is seen not only in the spin yields of the zero-neutron transfer channels at sufficiently high spins, but also in the spin yields of the transfer products over their entire spin population. For ^{48}Ca+^{176}Yb we present calculations that show that the flat slopes cannot be accounted for by direct Coulomb excitation of the transfer product or the population of the yrast band from excited bands. Our results differ somewhat from those of Takai *et al.* [4] in that we provide evidence of a deep inelastic component at sufficiently high spins in the zero- and few-neutron transfer products. This difference may stem from our use of heavier projectiles.

The comparative spin yield data do not support the need for a massive projectile to generate the angular momentum required to populate discrete states above the backbend in the rare-earth region. In fact, the smaller momentum of a lighter projectile results in less Doppler broadening and produces sharper γ-ray peaks. On the other hand, a light projectile may not be desirable for populating the most neutron-rich rare-earth isotopes since the driving force is then toward the neutron-deficient heavy fragments [6,18]. In such circumstances, to improve energy resolution, more highly segmented particle and/or segmented germanium detectors may be preferred in conjunction with a heavy projectile.

ACKNOWLEDGMENTS

We would like to express our gratitude to the staff of the 88-Inch Cyclotron for the development of the ^{154}Sm beam used in both ^{154}Sm+^{176}Yb and ^{154}Sm+^{208}Pb experiments. This work was supported in part by the U.S. Department of Energy under Contract No. DE-AC03-76SF00098.

[1] V.V. Volkov, Phys. Rep. **2**, 93 (1978).
[2] P. Glässel, R.S. Simon, R.M. Diamond, R.C. Jared, I.Y. Lee, L.G. Moretto, J.O. Newton, R. Schmitt, and F.S. Stephens, Phys. Rev. Lett. **38**, 331 (1977).
[3] R. Regimbart, A.N. Behkami, G.J. Wozniak, R.P. Schmitt, J.S. Sventek and L.G. Moretto, Phys. Rev. Lett. **41**, 1355 (1978).
[4] H. Takai *et al.*, Phys. Rev. C **38**, 1247 (1988).
[5] I. Y. Lee *et al.*, Phys. Rev. C **56**, 753 (1997).
[6] S.J. Asztalos *et al.*, Phys. Rev. C (submitted).
[7] R. Bass, *Nuclear Reactions with Heavy Ions* (Springer, New York, 1980).
[8] D.C. Radford, Nucl. Instrum. Methods Phys. Res. A **361**, 297 (1995).
[9] A. Johnson, H. Ryde, and J. Sztarkier, Phys. Lett. **12B**, 605 (1971).
[10] R. Bengtsson and S. Frauendorf, Nucl. Phys. **A314**, 27 (1979).
[11] R. Bengtsson, S. Frauendorf, and F.-R. May, At. Data Nucl. Data Tables **35**, 15 (1986).

[12] *Table of Isotopes*, edited by R.B. Firestone and V. S. Shirley (Wiley, New York, 1995), p. 5895.
[13] S.J. Zhu *et al.*, J. Phys. G **21**, L57 (1995).
[14] S.Y. Chu, J.O. Rasmussen, M.A. Stoyer, L.F. Canto, R. Donangelo, and P. Ring, Phys. Rev. C **52**, 685 (1995).
[15] S.Y. Chu, J.O. Rasmussen, M.A. Stoyer, P. Ring, and L.F. Canto, Phys. Rev. C **52**, 1407 (1995).
[16] S.Y. Chu, Ph.D. thesis, Yale University, 1993.
[17] J.O. Rasmussen, S.Y. Chu, M.A. Stoyer, L.F. Canto, R. Donangelo, and P. Ring, Phys. Rep. **264**, 325 (1996).
[18] S.J. Asztalos, Ph.D. thesis, University of California, Berkeley, 1998, Lawrence Berkeley National Laboratory Report No. 41895.